Time-Resolved Evolution of Short- and Long-Range Order During the Transformation of Amorphous Calcium Carbonate to Calcite in the Sea Urchin Embryo

*Chantel C. Tester, Ching-Hsuan Wu, Minna R. Krejci, Laura Mueller, Alex Park, Barry Lai, Si Chen, Chengjun Sun, Mahaling Balasubramanian, and Derk Joester**

Use of amorphous precursors is a widespread strategy in biomineralization. In sea urchin embryos, controlled transformation of amorphous calcium carbonate (ACC) to calcite results in smoothly curving and branching single crystals. However, the mechanism of the disorder-to-order transformation remains poorly understood. Here, the use of strontium as a probe in X-ray absorption spectroscopy (XAS) greatly facilitates investigation of the evolution of order. In pulse-chase experiments, embryos incorporate Sr^{2+} from Sr-enriched seawater into small volumes of the growing endoskeleton. During the chase, the Sr-labeled mineral matures under physiological conditions. Based on Sr *K*-edge spectra of cryo-frozen whole embryos, it is proposed that the transformation occurs in three stages. The initially deposited calcium carbonate has short-range order resembling synthetic hydrated ACC. Within 3 h, the short-range order of calcite is established. Between 3 h and 24 h, the short-range order does not change, while long-range order increases. These results refute the notion that organisms imprint the local order of the final crystal on ACC. Furthermore, it is proposed that the intermediate is more similar to disordered calcite than to anhydrous ACC. Pulse-chase experiments in conjunction with heavy element labeling have great potential to improve understanding of phase transformations during biomineralization.

1. Introduction

The biological use of amorphous precursor minerals is thought to be directly related to the unparalleled ability to create single crystalline, yet composite biominerals with intricate shapes.[1] Despite considerable effort in recent years, it has not been possible to capture the mechanistic detail of the disorder-to-order transformation that is the key element of this process. This is due to the challenges of characterizing the structure of the mineral precursors, which lack long-range order and are unstable toward crystallization. Efforts to characterize their transformation have utilized synchrotron X-ray techniques such as X-ray aborption spectroscopy (XAS),[2–5] pair distribution function (PDF) analysis,[4,6] and X-ray photoelectron emission microscopy (X-PEEM),[7,8] to obtain detailed structural information at the atomic scale. While progress has been made studying synthetic amorphous precursors that can be prepared as bulk powders,[4,6,9,10] characterization of the transformation in vivo presents considerable challenges. These include the small weight fraction of mineral in samples, the microscopic size of mineral precipitates, and the presence of multiple phases and metastable intermediates. In previous attempts to characterize biogenic amorphous precursors, it has been necessary to harvest the mineral from the organism to ensure adequate signal strength at sufficient spatial and temporal resolution. As metastable intermediates are highly prone to undergo phase transformations during such sample preparation, the resulting data rarely reflect physiological states and have to be interpreted with great caution. In the following, we will consider what is arguably the most intensively studied model system for the use of amorphous precursors in biomineralization, namely the formation of the endoskeleton in the sea urchin embryo.

Sea urchins make masterful use of ACC in the synthesis of intricately shaped endoskeletal elements in all stages of their development.[11] The embryonic endoskeleton consists of two mirror-symmetric spicules comprised of single crystalline calcite and embedded proteins.[12] The biomineral is commonly described as high magnesian calcite, with as much as 5 mol% of Ca^{2+} sites substituted with Mg^{2+}.[13,14] Spicule synthesis commences with the formation of a calcareous granule, which is elongated parallel to the crystallographic *a*-axes into the triradiate rudiment (**Scheme 1**). At characteristic times during subsequent development, two of the radii change growth direction by 90° (from *a*- to *c*-axis). Further growth and additional branching events result in the mature endoskeleton. The

C. C. Tester, C.-H. Wu, Dr. M. R. Krejci,
L. Mueller, A. Park, Prof. D. Joester
Department of Materials Science and Engineering
Northwestern University
Evanston, IL 60208, USA
E-mail: d-joester@northwestern.edu
Dr. B. Lai, Dr. S. Chen, Dr. C. Sun,
Dr. M. Balasubramanian
Advanced Photon Source
Argonne National Laboratory
Argonne, IL 60439, USA

DOI: 10.1002/adfm.201203400

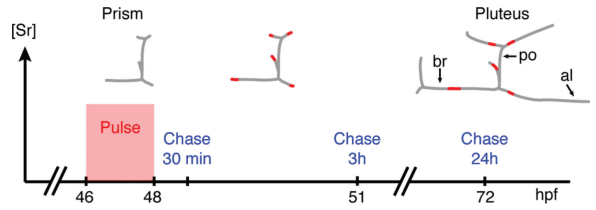

Scheme 1. Scheme of the pulse-chase experiment for incorporating Sr into the developing *Lytechinus pictus* larval spicules. Above, the schematic representation of spicules at different stages (i.e., prism and pluteus) correspond to the developmental timeline. br = body rod, po = postoral rod, al = anterolateral rod.

synthesis of spicules is carried out collaboratively and rapidly (5–13 $\mu m \cdot h^{-1}$) by primary mesenchyme cells that have fused their plasma membranes to form a syncytium.[15] Spicule growth has been shown to proceed through amorphous calcium carbonate precursors.[5,7,8,10,16] Mineral deposition occurs in a membrane-delimited environment inside the cells, that is not in contact with the outside medium.[16]

To characterize short-range order during the transformation from ACC to calcite, Politi and co-workers employed XAS at the Ca *K*-edge. Data were initially collected from whole embryos at cryogenic temperature, thus capturing the mineral under conditions very close to those in the live embryo.[5] While X-ray absorption near edge structure (XANES) analysis qualitatively demonstrated the change in local order of spicules over time, quantitative analysis of the extended X-ray absorption fine structure (EXAFS) was only possible after separating spicules from the organism. This, however, was reported to lead to uncontrolled transformation of metastable material during sample preparation.[5] A second fundamental problem of EXAFS of whole embryos is that calcium in the entire volume of the spicule is probed at different developmental stages. As the relative proportion of newly deposited material becomes smaller with increasing size, any analysis is biased towards detecting the final, ordered calcite.

To address this problem, Politi and Gilbert analyzed extracted spicules using X-PEEM, a surface sensitive technique with high spatial resolution.[8] Ca *L*-edge XANES spectra extracted from X-PEEM data differ qualitatively in the intensity and width of crystal-field satellite peaks of the Ca L_2- and L_3-edge. Based on a linear combination of spectra of two synthetic reference compounds and a hypothetical intermediate, the authors propose the co-existence of three forms of calcium carbonate, namely, short-lived hydrated ACC (ACC-I), less disordered and more stable anhydrous ACC (ACC-II, see also ref. [10]), and calcite. In spicule cross-sections, the most disordered material (ACC-I) predominates at the spicule surface, but also occurs in the form of occluded islands in the interior. Calcite and the intermediate (ACC-II) constitute the bulk of the spicule.[7] Importantly, the structure of the spicule appears granular, where the relative amount of the three phases changes over distances as small as 40 nm. While X-PEEM offers unrivaled in-plane resolution, XANES generally does not allow a quantitative analysis of local order and is highly dependent on the availability of meaningful reference compounds. In biogenic systems, this can be a significant challenge.

In an attempt to connect structural models with XANES data, Rez and Blackwell employed crystal field calculations to simulate the Ca L_{23}-edge spectra recorded by Gilbert and co-workers.[17] They find that one way to simulate XANES-spectra of the two postulated forms of ACC is by distorting the nearest-neighbor coordination polyhedron from the (idealized) octahedron in calcite. Interestingly, they propose that the transition from ACC-I to ACC-II involves polyhedra aligning along the *z*-direction with no changes in local order. The transformation from ACC-II to calcite then occurs with further alignment in the *x*–*y* plane and changes in the local order. While the approach is promising, the model does not capture the multitude of different coordination environments of Ca in ACC that for example Reeder and co-workers find using pair distribution function analysis of total scattering data.[4] Given that the Ca L_{23}-edge spectra are very sensitive to changes in geometry,[17] the structure proposed by Blackwell and Rez may just be one of many that gives rise the to spectra observed by Gilbert and co-workers. Finally, some concerns remain about the influence of sample preparation needed for X-PEEM, which include extraction of spicules, resin embedding, grinding and polishing, and analysis at high vacuum.

It is thus desirable to use an analytical technique that can be performed without harvesting spicules from the embryo, yet has sufficient sensitivity to allow quantitative determination of local and long range order. Furthermore, it would be advantageous to be able to probe small volumes rather than whole spicules. Herein, we use strontium as a spectroscopic probe for XAS to obtain local structural information. Strontium and calcium are both alkaline earth metals and exhibit similar chemical properties. Most importantly, they both occur as divalent cations with similar effective ionic radii. As a consequence, Sr^{2+} can substitute for Ca^{2+} in calcium carbonate. Using X-ray fluorescence microscopy, we show that when sea urchin embryos are exposed to elevated Sr^{2+} in the medium during a pulse period, followed by a chase period in Sr^{2+}-free medium, Sr^{2+} is incorporated into well-defined regions of the growing spicule. This provides the basis for Sr *K*-edge XANES and EXAFS analysis of the amorphous to crystalline transformation in the spicules of cryo-frozen embryos.

2. Results and Discussion

2.1. Sea Urchin Embryo Pulse-Chase Experiments

Lytechinus pictus embryos were generated by in vitro fertilization and cultured in artificial sea water (ASW containing 10 mM Ca^{2+}) following the procedure of Wilt.[18] At the prism stage (≈46 h post fertilization) embryos were transferred to Sr-enriched ASW (1 mM Sr^{2+}, 9 mM Ca^{2+}, Scheme 1). After a 2 h exposure (pulse), the culture medium was changed back to ASW (chase). Embryos were then harvested 30 min, 3 h, and 24 h from the start of the chase (corresponding to 2.5 h, 5 h, and 26 h after the addition of Sr). No changes in the development of the embryos were observed as a result of the strontium pulse.

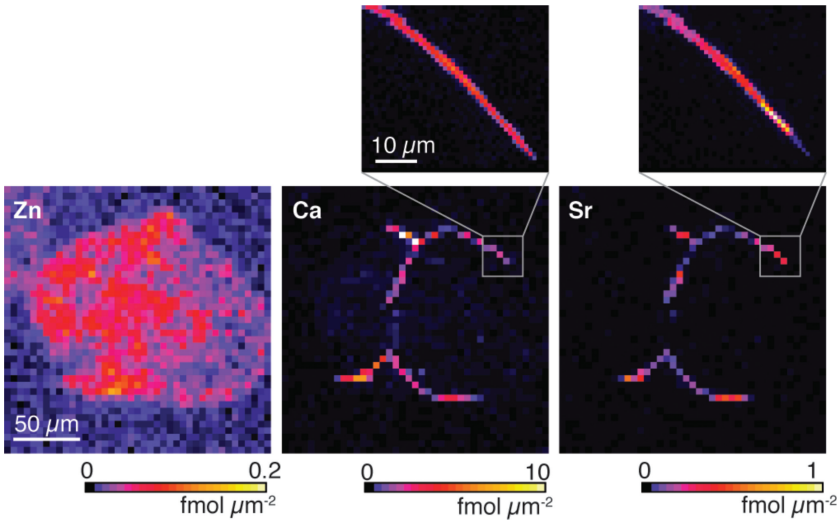

Figure 1. Zn, Ca, and Sr XFM maps of a frozen-hydrated sea urchin embryo, plunge frozen 3 h from the start of the chase. The Zn map outlines the entire embryo, the Ca map outlines the pair of $CaCO_3$ spicules, and the Sr map reveals the regions that have been Sr-labeled.

2.2. Sr Incorporation into the Growing Spicule

To identify regions labeled during the Sr-pulse, we performed low-resolution elemental mapping of labeled embryos using X-ray fluorescence microscopy (XFM). Whole sea urchin embryos were plunge frozen and stored in liquid nitrogen to preserve the embryos and prevent phase transformations prior to characterization. Samples were kept frozen during imaging using a liquid nitrogen cryo-jet. XFM elemental mapping was performed above the Sr *K*-edge, with the beam focused to a diameter of approximately 0.25 μm. We find that the distribution of Ca and Sr in the embryo is best analyzed by comparing Sr-, Ca-, and Zn-maps (**Figure 1**). While the former two are predominantly present in the endoskeleton, Zn is fairly uniformly distributed throughout the soft tissues.

Sr-maps indicate that Sr is incorporated thoughout the spicule, but in soft tissues is only present in negligible amounts (Figure 1). A small amount of Sr (area concentration ≈ 0.1 fmol μm^{-2}) is present in the biomineral formed prior to and after the embryo is exposed to Sr in the medium. This background level of Sr incorporation is likely due to Sr present as an impurity in Ca salts used to prepare ASW. While we expect calcium to be present in the soft tissues, the very high concentration of Ca in the biomineral dominates Ca-maps. We do not find features that are consistent with a substantial amount of calcium present in storage vesicles.[16] However, at the resolution at which the measurements were performed, we would not be able to detect storage vesicles that are very close to spicules. The experimental setup we used is not sensitive to fluorescence from low atomic number (*Z*) elements such as magnesium; we were thus unable to confirm the presence of Mg^{2+} in the spicule biomineral.[13,14]

An XFM image is a 2D projection of a 3D elemental distribution. While the volume concentration of Ca in the spicule is nearly constant, the angle between the spicule and the image plane, the spicule diameter, and spicules crossing each other can lead to the variations observed in the Ca area concentration map. To identify the regions that were labeled with Sr during the pulse, it is thus useful to search for areas where the Sr/Ca ratio is increased over the background value. We find that there are several such hot spots where the strontium concentration approaches 10% of the calcium concentration. This is in line with a study reporting up to 12.5% of Ca^{2+} ions replaced by Sr^{2+} in calcitic limpet shells, albeit these limpets were exposed to a culture medium with a fourfold higher Sr:Ca ratio of 1:1.1.[19]

In the closely related species *Lytechinus variegatus*, Guss and Ettensohn determined that spicule growth between prism and pluteus stages will primarily occur by elongation of the body rod (≈10 μm h^{-1}), the post-oral rod (≈13 μm h^{-1}), and the antero-lateral rod (≈6 μm h^{-1}).[15] We thus expected that during a 2 h pulse, Sr would be incorporated over 12–26 μm length, in three distinct places in each spicule. The distribution and size of the Sr hot spots are consistent with this expectation (Figure 1 and Scheme 1). We conclude that Sr is taken up from the medium during the pulse and is incorporated into small volumes of biomineral synthesized during this time. While we do not know the absolute concentrations or the Sr/Ca ratio of the solution that calcium carbonate is precipitated from within the cells, we observe that the Sr/Ca ratio in the final mineral is similar to that in the pulse medium. While Sr^{2+} can strongly affect the growth of calcite crystals from bulk solution,[20] it appears that biomineralization in the sea urchin embryo is not affected. Note the similar disparity between the very strong influence of the Mg^{2+} concentration on crystal growth and polymorph selection in bulk precipitation as compared to biomineral growth.[21] This disparity is most likely the combined effect of the specific conditions under which the biomineral is formed, namely confined in small volumes,[16,22] in the presence of organic macromolecules,[1] and via an amorphous precursor.

2.3. μ-XANES of Sr-Labeled Spicules

Immediately after elemental mapping by XFM, μ-XANES spectra (**Figure 2**) were acquired from those regions of the spicule that displayed the most intense Sr-labeling. The advantage of using a focused X-ray beam is that it enables structural characterization of select areas of the spicule, with minimal contributions from strontium elsewhere in the embryo. Spectra recorded from spicules harvested after a chase period of 30 min, 3 h, and 24 h all display a broad white line at E = 16,115 eV. A pronounced shoulder towards higher energy becomes visible at 3 h and develops into distinct second peak at E = 16,126 eV at 24 h.

Near edges features are sensitive to the coordination environment of the absorbing atom, in our case the first coordination shell around Sr^{2+}. As strontium ions are similar to, but not identical with calcium ions, it is important to consider possible

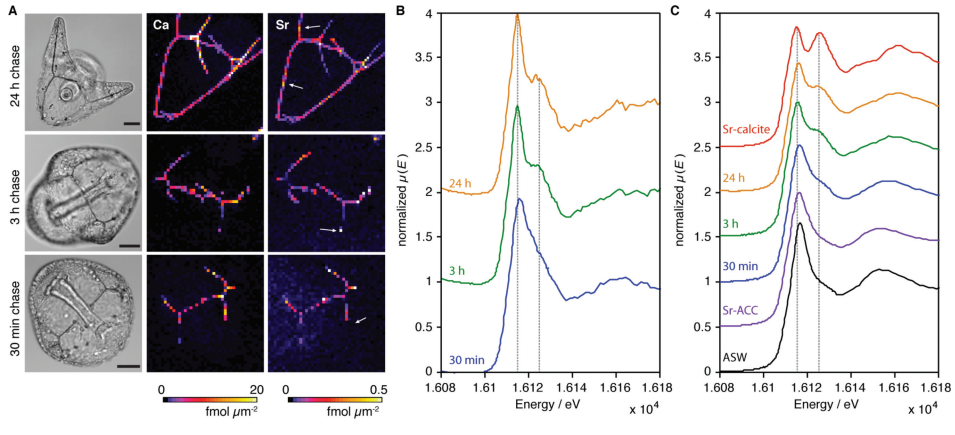

Figure 2. A) Light microscopy images (scale bar represents 50 μm) and Ca- and Sr-fluorescence maps of sea urchin larval spicules after 30 min, 3 h, and 24 h chase (2.5 h, 5 h, 26 h from start of Sr-pulse). Arrows indicate the Sr-labeled regions examined by μ-XANES. Similarity between μ-XANES data from B) Sr-labeled regions and C) XANES data measured from bulk suspensions of Sr-pulsed embryos demonstrate that absorbance arises primarily from the labeled regions.

outcomes of this substitution and the corresponding features we would expect in XANES spectra. The most important questions are whether there is a miscibility gap in the $(Ca,Sr)CO_3$ solid solution and whether any strontianite might be formed. A miscibility gap could result in the demixing of Sr-poor and Sr-rich phases. Strontianite, the Sr-rich endmember of the solid solution, has aragonite rather than calcite structure. While demixing and strontianite formation have not been observed in spicules grown in seawater with natural abundance of strontium (91 μmol kg^{-1}), it is in principle possible that at the much higher Sr levels in labeled spicules and/or in combination with Mg^{2+} present, the formation of an aragonitic structure might become favored. We are, however, confident, that this does not happen in the Sr-labeled spicules for three reasons. 1) The changes in the near edge features over the course of the chase are consistent with changes detected by Politi and co-workers in Ca *K*-edge XANES of developing embryos.[5] The emergence of the second peak at $E = 16{,}126$ eV in Sr *K*-edge μ-XANES is equivalent to that of the second peak in Ca *K*-edge XANES that marks the structural transformation of ACC to calcite. This peak is absent from the Sr-*K*-edge XANES spectra of strontianite (Supporting Information Figure 4). Given that the Sr *K*-edge spectrum of strontianite is almost perfectly identical to that of Sr-substituted aragonite,[23] the absence of the peak at $E = 16{,}126$ eV demonstrates that neither is present in the spicule. 2) The spicules appear normal and develop normal birefringence as they mature (see Section 2.5). This is evidence against the formation of a second crystalline phase. 3) In the far edge region, linear combination fitting of Sr-ACC, Sr-calcite, and strontianite standards to *k*-space spectra indicate the complete absence of strontianite (Supporting Information Figure 5). We therefore conclude that Sr is homogenously distributed in the labeled biomineral, forming a solid solution, and can be used to probe the structural evolution of the labeled biomineral. Further, at the resolution of the experiment, the presence of Sr does not appear to significantly affect the kinetics of the phase transformation.

While Sr- and Ca-*K*-edge XANES spectra of the evolving spicules share many similarities, we also observed some differences. These arise primarily from the shorter core-hole lifetime of strontium.[24] For example, during the early stages of spicule growth, shifts in the Ca *K*-edge corresponding to changes in the Ca-O coordination number were detected, but cannot be resolved at the Sr *K*-edge.[5] Additionally, the pre-edge peak in Ca *K*-edge XANES that is characteristic of distorted octahedral coordination geometry of Ca^{2+} in synthetic and biogenic ACC is absent in Sr *K*-edge XANES spectra (Figure 2). This is likely due to broadening of the pre-edge peak typical for 4d transition elements.[25]

Despite probing only ≈ 4 pg mineral in the path of the beam, μ-XANES is sufficiently sensitive to extract qualitative information regarding the evolution of the mineral structure in specific volumes over the course of the chase. However, low signal-to-noise ratio and sample drift prevent quantitative analysis of the far edge region. The advantage of the pulse-chase labeling approach is that Sr-labeled regions can be probed by bulk Sr-edge XAS without compromising spatial or temporal resolution.

2.4. Bulk X-Ray Absorption Spectroscopy of Whole Embryos

In addition to the benefits of probing the evolution of a particular volume over time, we expected that the use of strontium as a structural probe would also improve the signal-to-noise ratio compared to that in Ca *K*-edge bulk XAS. This is due to the higher absorption energy of strontium. Working at higher incident beam energy significantly reduces attenuation of incident and emitted X-rays. We anticipated that this might enable analyzing frozen-hydrated biological samples, where the attenuation by cryostat windows and a substantial layer of vitreous ice reduced the signal-to-noise of Ca-*K*-edge XAS spectra to the point where analysis of far edge features became impossible.[5]

For bulk cryo-XAS, samples were prepared by freezing concentrated suspensions of whole embryos in liquid nitrogen. Phase transformations were prevented by storing samples in liquid nitrogen prior to measurements and by mounting samples in a cryostat maintained at 90 K for the duration of the

XAS experiments. Powders of Sr-substituted calcite (Sr-calcite, 1.8% of Ca replaced by Sr) and Sr-substituted ACC (Sr-ACC, 12% of Ca replaced by Sr) were used as reference compounds.

Bulk Sr *K*-edge XANES spectra clearly show the evolution from Sr-ACC to Sr-calcite we observed in Sr *K* -edge μ-XANES, with a significantly improved signal-to-noise ratio (Figure 2). Spectra recorded 30 min into the chase show the characteristic, broad white line of Sr-ACC (E = 16 115 eV). At 3 h, a distinct shoulder develops that at 24 h turns into the peak at E = 16 126 eV that is characteristic for Sr-calcite. The intensity of this second peak is significantly more pronounced in Sr-calcite than after 24 h chase. This difference is most likely an indication that the phase transformation is not yet complete. However, the synthetic Sr-calcite we use as a reference imperfectly captures some aspects of the biogenic material, for instance the degree of Sr substitution, and others, such as substitution with Mg^{2+} and the presence of organic macromolecules, not at all. Limitations of this kind are typical for XAS analysis of biogenic materials and need to be considered when interpreting spectra.

There is high similarity between XANES spectra of Sr-ASW and Sr-ACC. In principle, this creates a problem in identifying biogenic Sr-ACC during the early time points. However, we are confident that signal in bulk XAS predominantly comes from Sr incorporated in the spicules during the pulse for the following reasons: 1) there is no detectable signal in XAS experiments performed on embryos that were not exposed to a pulse and that consequently only have background levels of Sr in the spicules (not shown); 2) there is virtually no Sr signal outside the spicules in XFM maps, indicating that the concentration of "free" Sr in the medium and the soft tissues of the embryo is negligible; and 3) there is very good agreement between μ-XANES and bulk measurements.

To analyze the far edge region of the spectra, XAS data was converted from energy into *k*-space, then Fourier-transformed into *R*-space (**Figure 3**). The resolution in *R*-space, which depends on the range of usable *k*-space data, is approximately 0.2 Å. The disorder-to-order transformation during spicule maturation is visible in both *k*-space and *R*-space. In *k*-space, spectra of Sr-ACC and spicules after 30 min chase show only one oscillation corresponding to scattering from the first nearest neighbor. In *R*-space, this corresponds to a single peak at ≈2 Å. After 24 h, higher frequency oscillations are apparent, resulting from scattering from more distant coordination spheres. In *R*-space, this corresponds to additional peaks at greater values of *R*. The peak at ≈4 Å in *R*-space spectra is a major feature beyond the first coordination sphere. Its intensity increases over the course of the chase and it is very pronounced in Sr-calcite. At the same time, a decrease in frequency of the primary oscillation in *k*-space corresponds to a shift of the peak at ≈2 Å towards smaller *R*. This is consistent with a decrease in first nearest neighbor bond distance from Sr-ACC to Sr-calcite. Taken together, these observations signify increasing long-range order, and increasing similarity to Sr-calcite.

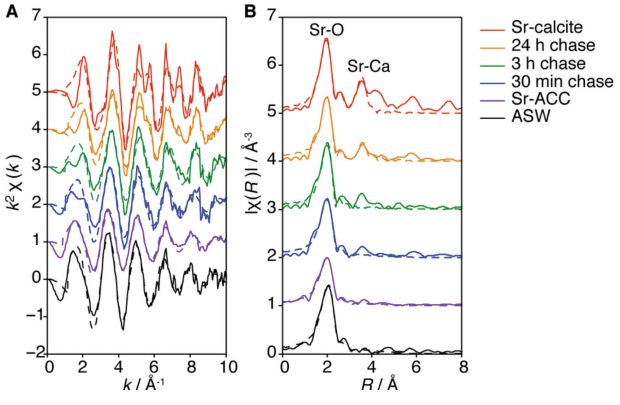

Figure 3. Sr *K*-edge EXAFS spectra in *k*-space (A) and *R*-space (B) recorded from bulk frozen-hydrated whole sea urchin embryos at different chase time points. Reference standards were recorded at cryogenic temperature. Spectra were fitted to models constructed from the scattering paths of calcite (dashed lines).

2.5. EXAFS Data Modeling

For a quantitative analysis of short-range order, the extended fine structure region was fitted to models constructed from the scattering paths of calcite. Theoretical phase shifts and scattering amplitudes were determined by considering an absorbing Sr^{2+} in place of a single Ca^{2+} in the calcite lattice.[26] The calculated scattering factors were then used to refine the structural parameters from our data, including the coordination number of strontium, bond lengths, and mean square disorder in bond lengths (Debye-Waller factor) of the neighboring atoms.

In a dilute solid solution of Sr^{2+} in $CaCO_3$, we expect the structure surrounding the Sr-impurities to dilate due to the larger effective ionic radius of Sr^{2+} (1.32 Å) compared to Ca^{2+} (1.14 Å).[27] Indeed, first shell Sr-O bond lengths of Sr-substituted calcite are dilated by 7% compared to unsubstituted calcite. The dilatory effect decreases progressively in successive coordination spheres, i.e., with increasing distance from the Sr-impurity (**Table 1**) and is consistent with Sr-EXAFS analysis of strontium-substituted geologic calcite.[23]

Table 1. Curve-fitting results of Sr K-edge EXAFS data from Sr-labeled sea urchin embryos and controls. *N*: coordination number, *R* (Å): distance from Sr, and σ^2 (Å^2): Debye-Waller factor. Complete and alternate fitting results are shown in Supporting Information.

Sample	Shell	*N*	*R* [Å]	σ^2 [Å^2]
Sr-calcite	Sr-O	6[a)]	2.52 (0.01)	0.006 (0.001)
	Sr-C	6[a)]	3.30 (0.04)	0.006 (0.004)
	Sr-O	6[a)]	3.47 (0.08)	0.02 (0.01)
	Sr-Ca	6[a)]	4.12 (0.01)	0.006 (0.001)
24 h chase	Sr-O	5.2 (0.7)	2.54 (0.01)	0.005 (0.001)
	Sr-Ca	2 (1)	4.11 (0.02)	0.002 (0.004)
3 h chase	Sr-O	5.4 (0.8)	2.54 (0.01)	0.004 (0.001)
30 min chase	Sr-O	6 (1)	2.57 (0.01)	0.008 (0.002)
Sr-ACC	Sr-O	6.4 (0.6)	2.60 (0.01)	0.010 (0.001)
ASW	Sr-O	9.4 (1.2)	2.64 (0.01)	0.011 (0.002)

[a)]Parameter fixed.

A systematic change in the nearest neighbor (Sr-O) bond distances over the course of the chase indicates a progressing structural transformation. Consistent with the decrease in frequency in *k*-space, the first-shell Sr-O bond length decreases from 2.57 ± 0.01 Å at 30 min to 2.54 ± 0.01 Å at 3 h (Figure 3, Table 1). No further change is observed between the 3 h and 24 h time points.

EXAFS modeling of the data from Sr-calcite further indicates that the peak at ≈ 4 Å is due to scattering from calcium in the fourth shell. Scattering from carbon in the second shell and oxygen in the third shell produces weaker and possibly overlapping peaks that are more difficult to fit. The ability to reliably fit peaks beyond the first nearest neighbor demonstrates the development of long-range order. At early time points, 30 min and 3 h from the start of the chase, the Sr-Ca coordination number could not be reliably fit, indicating that the initially deposited mineral is highly disordered. Yet even in the mature spicule at 24 h, the Sr-Ca coordination number is a low 2 ± 1. This suggests that the degree of order in the spicule is still less than that of synthetic calcite.[1,28]

While it is difficult to use EXAFS to precisely measure both the Sr-O coordination number and the coupled Debye-Waller factor, there is clear evidence for a disorder-to-order transformation over the course of the chase. The initially deposited mineral at 30 min has a short-range order that is distinctly different from Sr-calcite and is more similar to that of synthetic, hydrated Sr-ACC. By the 3 h time point, the mineral has adopted the short-range order of the mature mineral, with nearest neighbor bond lengths and mean-square disorder similar to Sr-calcite. Finally, by 24 h, order beyond the first nearest neighbor has emerged, suggesting that initially formed units with calcite short-range order have aligned into a lattice.

In contrast, Ca *K*-edge EXAFS suggested that the initially deposited amorphous mineral has short-range order similar to the mature crystal, and it was speculated that the organism might use organic macromolecules to "imprint" the final polymorph on the amorphous precursor.[1,3,5,28] The formation of a short-lived, hydrated ACC-I precursor on the spicule surface was first inferred by Politi and co-workers based on Ca L_{23}-edge XANES spectra recorded by X-PEEM. However, even with additional support from crystal field simulations by Rez and Blackwell, this interpretation was based on a qualitative comparison with reference spectra.[8,17] Also, some questions remained whether a short-lived, hydrated ACC could reasonably be expected to "survive" sample preparation and the high-vacuum conditions of X-PEEM. In comparison, the data from Sr *K*-edge EXAFS of cryo-frozen whole embryos we present herein unambiguously and quantitatively show that ACC does not have calcite short-range order at the 30-min mark. Interestingly, the short-range order of calcite is established by the 3 h mark. Between the 3 h and 24 h marks, the only change appears to be a gradual increase in long-range order. The question then becomes whether this is consistent with the proposal that the first-formed, hydrated ACC-I transforms into anhydrous ACC-II, as suggested by Gilbert and co-workers and observed in abiotic precipitation,[10,29] or whether the transformation results in disordered calcite. In the absence of a reference compound, interpretation of Ca L_{23}-edge XANES spectra associated with ACC-II is essentially speculative. It therefore appears prudent to consider the possibility that crystalline order develops earlier than currently assumed.

2.6. Birefringence as an Indicator of Crystalline Order

An experimentally straightforward approach to distinguish ACC from calcite is to establish whether the material is birefringent. In calcite, the speed at which light propagates depends on its direction of travel and the direction of its polarization. This is a consequence of the anisotropy of the calcite lattice and results in calcite exhibiting two indices of refraction, one for propagation parallel to the *c*-axis (optical axis) and one for any direction normal to the optical axis. Practically, this means that when the crystal is viewed between crossed polarizers in any direction but along its optical axis, and rotated 360° around the viewing direction, it will appear maximally dark every 90° (the extinguishing positions). It will appear maximally bright when rotated by 45° from an extinguishing position. A completely amorphous material such as ACC will appear dark independent of its orientation between polarizers. Mature, calcitic sea urchin embryo spicules show typical calcite birefringence.[14] To establish whether Sr-labeled regions are birefringent at the 3 h timepoint, a pulse-chase experiment was performed where sea urchins were co-labeled with a calcium-binding fluorophore, calcein, during the pulse (**Figure 4**). Both before and after removal of soft tissues, those regions of the spicules co-labeled by calcein and Sr are birefringent. In fact, birefringence is detected even in more recently deposited mineral. This is consistent with Beniash and co-workers observation that spicules isolated at the prism stage exhibit birefringence over their entire length.[16] When rotated between crossed polarizers, spicule birefringence is consistent with a continuous single crystal. The Sr-labeled zone does not behave differently than spicule mineral deposited prior to, or after the pulse. We interpret this to mean that at the 3 h chase time point, the mineral has lost its isotropic, amorphous character. Instead, it must have a significant degree of long-range order, which cannot be detected by EXAFS, but that gives rise to the observed birefringence. We propose that it may be more accurate to refer to this material as disordered calcite than as ACC.

2.7. Accounting for Multiple Phases: Linear Combination Fitting

Inherent to the above discussion of the change in local order of the mineral is the assumption that we are observing the slow transformation of structure in a homogenous solid. An alternative interpretation is that the changes in the near and far edge regions of the spectra are due to multiple forms of $CaCO_3$ present in varying amounts. Support for a heterogeneous microstructure of the spicule mineral at length scales as small as 20 nm comes from X-PEEM experiments by the Gilbert group.[7,8] The probe volumes in the Sr-edge XAS experiments described herein are typically greater than 30 μm^3 per spicule. It is thus entirely possible that the EXAFS spectra result from a linear combination of two or more components. Please note that, for lack of a better term, we use components here to encompass all phases in the strict sense, plus any metastable intermediates.

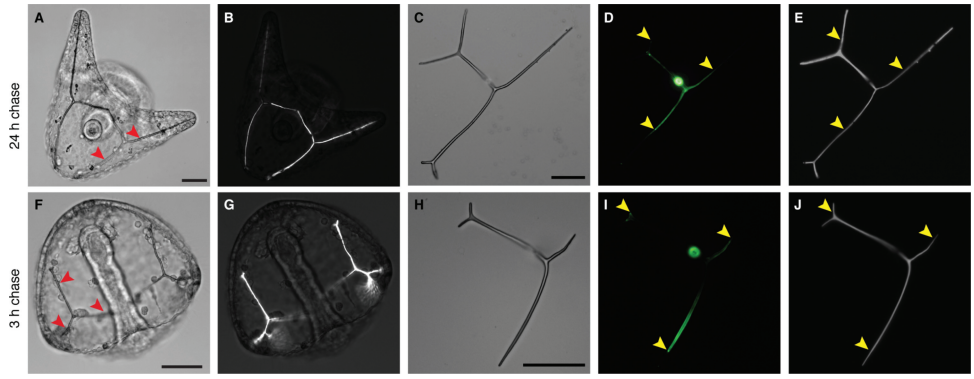

Figure 4. Sea urchin embryos at A–E) 24 h and F–J) 3 h after co-labeling with Sr and calcein. Based on the timing of the pulse, strontium/calcein incorporation is likely to occur at spots indicated by the red arrowheads (A,F). For comparison, see spicules after removal of cellular materials (C,H). Note that, in the live embryo, the entire spicule is birefringent in the polarized light at both stages (B,G). Autofluorescence from the whole embryo prevents visualization of calcein incorporation. After removal of the cellular materials, mineral deposited during and before the pulse can be visualized by calcein fluorescence (D,I). An abrupt drop in intensity occurs at the end of the pulse period, indicated by the yellow arrowheads. Note that the entire calcein-labeled region of the mineral is birefringent (E,J). Birefringence beyond the yellow arrowheads at 3 h chase (J) indicates that there is significant amount of order present even in mineral that has been deposited after the end of the pulse. Scale bar represents 50 µm.

This is different from the conventional use, where components are chemically distinct constituents of phases.

We first considered a two-component system, where metastable, hydrated Sr-ACC converts directly into Sr-calcite. To determine relative amounts of the two components at the different time points, we fitted a linear combination of EXAFS *k*-space spectra of the synthetic Sr-ACC and Sr-calcite standards to spectra from the whole sea urchin embryos (**Figure 5**). Under the assumptions of this model, it appears that in the Sr-labeled regions, the fraction of Sr-ACC decreases by almost a factor of two between the 30 min and the 24 h chase time points (from 73 ± 2%, *R*-factor = 0.10, χ^2 = 3.3 to 38 ± 2%, *R*-factor = 0.10, χ^2 = 3.5). While the 3 h chase time points follows this trend (53 ± 2% Sr ACC, 47 ± 2% Sr-calcite), a relatively poor fit is obtained (*R*-factor = 0.13, χ^2 = 5.2), suggesting that the structure of the mineral phase is poorly described by the synthetic reference compounds. The poor fit notwithstanding, this model is consistent with the observed development of birefringence in spicules very early on: ≈27% of the newly deposited Sr-ACC has transformed into crystalline calcite by the 30 min timepoint, i.e., within 2.5 h from the beginning of the pulse. However, the transformation of hydrated Sr-ACC appears much slower than what the interpretation of X-PEEM data by Gilbert and co-workers suggest.[7,8]

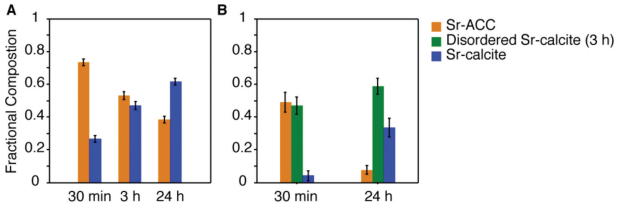

Figure 5. Results of linear combination fitting. A) The amorphous to crystalline transformation is detected in the fitting of $k^2\chi(k)$ data of Sr-calcite and Sr-ACC reference compounds (two component model) to data recorded over the course of Sr-chase (30 min, 3 h, and 24 h). B) A three-component model was generated by including the data from the 3 h chase time point in the fitting of data for the 30 min and 24 h chase time points. Complete fit results are shown in Supporting Information.

We therefore also considered a three-component model, similar to the one introduced by Gilbert and co-workers.[7,8] In addition to Sr-ACC and Sr-calcite, we assume that a third, intermediate stage exists. We use the EXAFS *k*-space spectrum of the 3 h timepoint as a standard for this component. Based on the birefringence at 3 h, we identify this material as a disordered calcite rather than as ACC-II.

Under the assumptions of this model, it appears that approximately one half of the initially deposited, hydrated Sr-ACC (49 ± 6%) has converted into disordered Sr-calcite (47 ± 5%) by the 30-min mark. Compared to this rapid transformation of ACC, in the same timeframe only traces of Sr-calcite are formed (4 ± 3%). By definition, conversion of Sr-ACC to the intermediate, disordered calcite is complete at 3 h. The transformation of the intermediate to Sr-calcite is very slow, with 59 ± 5% intermediate and 33 ± 3% Sr-calcite present at 24 h. The model indicates that a small amount of residual Sr-ACC (8 ± 6%) may still be present at this time. The improvement in the quality of the fit of the three-stage model relative to the two-stage model (30 min: *R*-factor = 0.07, χ^2 = 2.3, 24 h: *R*-factor = 0.05, χ^2 = 2.0) indicates that a three-component model better describes the amorphous to crystalline transformation in spicules.

However, accuracy of the linear combination fitting results depends greatly on the availability of meaningful reference compounds that accurately reflect the structure of the components. For example, while the results of the three-component linear combination are consistent with the results of Gilbert and co-workers, closer inspection reveals a contradiction to our assumption that the data collected at the 3 h chase time point is a homogenous component. Since the transformation of ACC is an energetically downhill sequence,[10] if Sr-calcite is present at 30 min, it must also be present at 3 h. Additionally, if low levels of Sr-ACC persist after 24 h, Sr-ACC must also be present at 3 h. While the amounts of the "offending" components predicted by linear combination fitting are small and the error substantial, we take this to indicate that the probe volume is not a homogenous component at 3 h.

Nevertheless, this model captures the high rate at which hydrated ACC is thought to transform into an intermediate form and is consistent with the early development of birefringence. As a three-component system, it is also consistent with the nanogranular architecture of the biomineral. Despite the obvious weakness that the 3 h time point is a somewhat arbitrarily chosen standard, we favor this model, as it is consistent with observations made by several independent techniques. The key difference between the model proposed herein and the one proposed by Gilbert and co-workers is that we identify the intermediate phase as having sufficient order to exhibit birefringence, hence disordered calcite, whereas Gilbert proposes that it is amorphous (ACC-II).

3. Conclusions

Understanding the evolution of structure from precipitation of an amorphous calcium carbonate precursor to the final biomineral in the sea urchin embryo remains a challenging goal. We have shown herein that on exposure of sea urchin embryos to Sr^{2+} in pulse-chase experiments, small, well-defined volumes of their spicules are labeled with the metal. The development of the embryos and the growth of the spicules are not affected by the presence of Sr in the medium or in the biomineral. By polarized light microscopy, Sr *K*-edge μ-XANES, and bulk Sr *K*-edge EXAFS, there is no indication for changes in the phase composition or the kinetics of the phase transformation in the spicule as a result of up to 10% substitution of the calcium ions with Sr^{2+}. The introduction of strontium as a probe into the calcium carbonate biomineral allows performing XAS at the Sr *K*-edge rather than at lower energy Ca *K*-edge. This has numerous advantages that stem from the increased absorption cross-section of strontium and the higher energy of the incident and emitted X-rays. Most importantly, the quality of data is sufficient for EXAFS analysis of spectra recorded from whole, frozen-hydrated embryos. In combination, this approach preserves the organism and the biomineral in a pristine state, preventing uncontrolled transformation of metastable or transient components, and allows probing the structural evolution of specific volume elements over time.

The transformation from amorphous precursor with distinct short-range order to the mature, calcitic biomineral is qualitatively apparent in near edge and far edge features of the Sr *K*-edge. Quantitative interpretation of EXAFS spectra is highly model-dependent, and requires assumptions with respect to the number and identity of components that contribute to the spectra. We favor a three-component model that is based on a linear combination of Sr-ACC, disordered Sr-calcite, and Sr-calcite reference spectra. Under the assumptions of this model, we observe that the initially deposited mineral is amorphous and similar in structure to hydrated synthetic ACC. The amorphous mineral is short lived, and rapidly transforms into an intermediate with calcite short range order, but reduced long-range order. Based on the birefringence of the spicule at the intermediate stage, we identify this component as disordered calcite. The transformation of disordered calcite into the final, mature biomineral is slow compared to the transformation of ACC. This model shares several aspects with that of Gilbert and co-workers,[7,8,10] but recognizes for the first time the distinct local order of the first formed amorphous phase and accounts for the birefringence of the spicule mineral at early times.

While there is currently little evidence that the presence of Sr^{2+} perturbs biomineralization in vivo, its influence on in vitro crystal growth is clear.[20] Therefore, we will need to further investigate how heavy element substitution might influence mineralization processes in vivo and in vitro. We envision that the improved sensitivity, the ability to study structural evolution over time, and the ability to investigate frozen-hydrated samples provided by heavy element spectroscopic probes will greatly aid studying biomineralization in situ, i.e., without drying or removal of soft tissues. In combination with complementary techniques, we are confident that our approach will help reconcile structural models of a range of poorly understood intermediates that have been postulated for the formation of crystalline polymorphs of calcium carbonate. These include anhydrous ACC-II in the sea urchin spicule,[7,8,10] proto-crystalline amorphous phases in *in vitro* precipitation,[9] and the disordered calcite phase we propose here.

4. Experimental Section

Materials: NaCl, KCl, $MgSO_4$, NaOH, $NaHCO_3$, and $Na_2CO_3{\cdot}H_2O$ (Mallinckrodt Baker Inc, Phillipsburg, NJ); MgCl2 · 6 H_2O (BDH, West Chester, PA); $SrCl_2{\cdot}6H_2O$ (Alfa Aesar, Ward Hill, MA). HNO_3 (EMD Millipore, Billerica, MA). ICP-MS standards (Inorganic Ventures, Christianburg, VA), Calcein (Sigma Aldrich, St. Louis, MO), 10–14% (w/v) sodium hypochlorite solution (BDH, West Chester, PA). All solutions were prepared with ultrapure water (ρ = 18.2 MΩ cm) using a Barnstead NanoDiamond UF+UV purification unit. Artificial seawater was prepared with the following concentration: 0.48 M NaCl, 0.01 M KCl, 0.027 M $MgCl_2$, 0.03 M $MgSO_4$, 0.01 M $CaCl_2$, and 0.002 M $NaHCO_3$. Sr-containing seawater (Sr-ASW) was prepared as ASW but with 0.009 M $CaCl_2$ and 0.001 M $SrCl_2$. Calcein was prepared as a 2.0 mg mL^{-1} stock solution in ASW, pH 8.3, and stored at 4 °C

Preparation of Sr-Labeled Sea Urchin Larval Spicules: *Lytechinus pictus* were purchased from Marinus Scientific, Garden Grove, CA. Collection of gametes and embryo culture was based on a published procedure.[18] Following in vitro fertilization, the embryos were cultured in ASW at 15 °C until the prism larval stage (ca. 46 h post fertilization, hpf), at which time the culture medium was changed to Sr-ASW (pulse). After a 2-h-pulse period, the embryos were transferred back to ASW (chase).

For X-ray fluorescence microscopy, live embryos were collected by centrifugation at 30 min, 3 h, and 24 h time points after the beginning of the chase period. Suspensions of embryos in the ASW medium were pipetted onto silicon nitride windows, and excess solution wicked onto filter paper before plunge freezing into liquid ethane.

For bulk XAS, larval spicule samples were prepared similar to Politi et al.[5] At 30 min, 3 h, and 24 h-chase period, live embryos were collected by centrifugation (2 min at 750 rpm, 15 °C). Excess ASW was removed by aspiration and replaced with 50% glycerol solution to minimize formation of crystalline ice. After further centrifugation, the embryo paste was filled into the window of a 3 mm thick copper sample holder and sealed with Kapton tape. The entire sample holder was then quickly frozen in liquid nitrogen, and stored in liquid nitrogen until XAS measurement.

Preparation of Sr-Enriched Standards: Sr-ACC was prepared according the Koga method.[30] Briefly, an aqueous solution of Na_2CO_3 (20 mL, 50 mM, pH = 13) and of an aqueous solution (10 mL) of $CaCl_2$ (90 mM) and $SrCl_2$ (10 mM) were chilled at –25 °C. After 1 h the solutions were thawed and rapidly mixed. The resulting precipitate was filtered and dried under vacuum for 30 min. Inductively coupled plasma mass

spectrometry indicates that 12% of the calcium sites are strontium substituted.

Sr-substituted calcite was prepared from a 9:1 mol ratio of calcium carbonate and strontium carbonate powders.[31] The powders were dissolved in ultra-pure water by bubbling carbon dioxide through for 48 h. The solution was then filtered and degassed by placing under vacuum for 24 h. The resulting Sr-calcite precipitate was filtered and vacuum dried. X-ray diffraction confirms that the precipitate is calcite with no evidence of vaterite, aragonite, or strontianite (Supporting Information Figure 3). Inductively coupled plasma mass spectrometry indicates that 1.8% of the calcium lattice sites are strontium substituted.

Powder samples were spread over Kapton tape for XAS characterization.

X-Ray Fluorescence Microscopy and μ-XANES: XFM mapping and μ-XANES was performed at beamline 2-ID-D of the Advanced Photon Source at Argonne National Laboratory. XFM is similar to the electron microprobe:[32] incident X-rays (or electrons) are focused on a sample, leading to the ejection of inner-shell electrons. Higher-shell electrons then fill the vacancies, resulting in the emission of X-rays that are characteristic of elements within the sample. XFM is particularly advantageous for elemental mapping of thick samples such as whole cells or embryos.[33]

Sea urchin embryos frozen on silicon nitride windows were transferred to aluminum sample holders under liquid nitrogen. The sample holders were then mounted in the path of a liquid nitrogen cryo-jet operating at 90 K stream temperature. XFM mapping was performed at 16.14 keV. Embryos were located by their characteristic appearance in Zn maps derived from low-resolution overview scans (500 μm × 500 μm, 10 μm step size, 0.5 s dwell time). Intermediate resolution scans of individual embryos (200 μm × 200 μm, 5 μm step size, 0.5 s dwell time) were used to identify spicules on Ca and Sr maps. Finally, high-resolution maps of Sr-labeled region of the skeleton were determined (0.5–1 μm step size) to identify suitable areas for μ-XANES.

μ-XANES spectra were recorded from regions of the spicule exhibiting the most intense Sr-labeling in XFM maps. To minimize the effects of sample drift during an energy scan caused by the cryo-jet, the zone plate was moved upstream by 1 mm prior to XANES scans, increasing the spot size to approximately 1 μm in diameter. Energy scans were acquired at the Sr K-edge with 0.5–1 eV step and 0.5–1 s dwell time, with a total range of 120 eV. Spectra were normalized to the absorbance of one X-ray by dividing by the edge jump.

Bulk X-Ray Absorption Spectroscopy: Bulk XAS was performed at beamline 20-BM-B of the Advanced Photon Source at Argonne National Laboratory. Concentrated suspensions of frozen embryos were transferred to a cryo-stat maintained at 90 K for the duration of the measurements. The Si(111) monochromator was calibrated by assigning an energy of 17 995.88 eV to the first peak in the derivative of the absorption edge of a Zr metal foil. Absorption spectra were recorded at the Sr *K*-edge using a 13-element Ge solid state detector in fluorescence geometry. Data was collected with 0.3 eV step size in the near edge region and with a 0.05 $Å^{-1}$ step size in the far edge region.

The data was normalized and background subtracted using Autobk, implemented in Athena.[34] χ-data were weighted by k^2 and the range prior to Fourier transformation optimized between $2.0 < k < 11.8$ Å. Fitting of the data to the crystal structure of Sr-substituted calcite was performed using Artemis.[34] The theoretical photoelectron scatting amplitudes and phase shifts were calculated using FEFF1. To generate the feff.inp file, which contains a list of the atomic coordinates centered at the absorbing atom, Atoms was used to calculate the atomic coordinates of calcite centered at Ca.[35] The list of atomic coordinates was then edited to replace the absorbing Ca atom with Sr. All neighboring calcium atoms remained unchanged. The total theoretical $\chi(k)$ for each model was then constructed from the most important scattering paths and fit in *R*-space. Multiple scattering was initially considered in fits to the Sr-calcite reference compound, but did not improve the quality of the fit, and was therefore omitted in all models. To reduce the number of variables against which data were fitted, the amplitude reduction factor (S_0^2) was estimated to be 1.2 by fixing the coordination numbers of the Sr-calcite reference compound to those known for pure calcite. This value was assumed to be the same for all scattering paths and fixed in all subsequent fitting schemes. While maintaining sufficient number of degrees of freedom, as defined by the Nyquist criterion, the coordination number, bond distance, Debye-Waller factor, and shift in energy origin were allowed to float. The validity of the fits was determined by the *R*-factor, and was minimized to ≤0.02.

Inductively Coupled Plasma Mass Spectrometry (ICP-MS): The Ca/Sr ratio in the Sr-calcite and Sr-ACC reference compounds was measured using a ThermoFisher X Series II ICP-MS (Thermo Scientific, Waltham, MA). The Ca and Sr concentrations were calibrated from standards prepared from commercially available stock solutions. Powders were dissolved in concentrated nitric acid, and then diluted to bring the Ca/Sr concentrations to within the 0–300 ppb range covered by the calibration curve. An internal standard of 5 ppb of scandium was added to each sample and standard to correct for matrix effects.

Calcein Labeling: Embryos were generated as described in the previous section. In order to observe the Sr-labeled regions by optical microscopy, the culture medium was changed at 46 hpf, from ASW to Sr-ASW containing the calcium binding fluorophore, calcein (100 μg mL^{-1}). After a 2-h-pulse period, the embryos were washed with ASW three times, and then transferred back to ASW.

For spicule extraction at 3 h and 24 h chase time points, embryos were transferred and incubated in 5–7% (w/v) sodium hypochlorite solution (bleach) for 10 min to remove the organic matter. After the incubation period, spicules were transferred to an Eppendorf tube and sedimented by centrifugation. Spicules were then washed once each with bleach, 30 mM Na_2CO_3, and 7.7 mM Na_2CO_3 solutions, then dehydrated with in an ascending series of ethanol solutions in water (30% (v/v), 50% (v/v), 75% (v/v), absolute ethanol). Spicules suspended in a drop of absolute ethanol were deposited on a glass slide and imaged in a Leica DMI6000B microscope equipped with polarized light and fluorescence optics.

Supporting Information

Supporting Information is available from the Wiley Online Library or from the author.

Acknowledgements

This work was supported in part by the US National Science Foundation (DMR-0805313 and DMR-1106208), the International Institute for Nanotechnology, and the MRSEC program of the National Science Foundation (DMR-1121262) at the Materials Research Center of Northwestern University (NU). PNC/XSD facilities at the Advanced Photon Source, and research at these facilities, are supported by the US Department of Energy - Basic Energy Sciences, a Major Resources Support grant from NSERC, the University of Washington, the Canadian Light Source and the Advanced Photon Source. Use of the Advanced Photon Source, an Office of Science User Facility operated for the U.S. Department of Energy (DOE) Office of Science by Argonne National Laboratory, was supported by the U.S. DOE under Contract No. DE-AC02-06CH11357. ICP-MS was performed at the Northwestern University Quantitative Bioelemental Imaging Center supported by NASA Ames Research Center NNA06CB93G.

Received: November 20, 2012
Revised: February 11, 2013
Published online: March 27, 2013

[1] L. Addadi, S. Raz, S. Weiner, *Adv. Mater.* **2003**, *15*, 959.
[2] Y. Levi-Kalisman, S. Raz, S. Weiner, L. Addadi, I. Sagi, *J. Chem. Soc. Dalton Trans.* **2000**, 3977.

[3] Y. Levi-Kalisman, S. Raz, S. Weiner, L. Addadi, I. Sagi, *Adv. Funct. Mater.* **2002**, *12*, 43.
[4] F. M. Michel, J. MacDonald, J. Feng, B. L. Phillips, L. Ehm, C. Tarabrella, J. B. Parise, R. J. Reeder, *Chem. Mater.* **2008**, *20*, 4720.
[5] Y. Politi, Y. Levi-Kalisman, S. Raz, F. Wilt, L. Addadi, S. Weiner, I. Sagi, *Adv. Funct. Mater.* **2006**, *16*, 1289.
[6] A. L. Goodwin, F. M. Michel, B. L. Phillips, D. A. Keen, M. T. Dove, R. J. Reeder, *Chem. Mater.* **2010**, *22*, 3197.
[7] Y. U. T. Gong, C. E. Killian, I. C. Olson, N. P. Appathurai, A. L. Amasino, M. C. Martin, L. J. Holt, F. H. Wilt, P. Gilbert, *Proc. Natl. Acad. Sci. USA* **2012**, *109*, 6088.
[8] Y. Politi, R. A. Metzler, M. Abrecht, B. Gilbert, F. H. Wilt, I. Sagi, L. Addadi, S. Weiner, P. Gilbert, *Proc. Natl. Acad. Sci. USA* **2008**, *105*, 20045.
[9] D. Gebauer, P. N. Gunawidjaja, J. Y. P. Ko, Z. Bacsik, B. Aziz, L. J. Liu, Y. F. Hu, L. Bergstrom, C. W. Tai, T. K. Sham, M. Eden, N. Hedin, *Angew. Chem. Int. Ed.* **2010**, *49*, 8889.
[10] A. V. Radha, T. Z. Forbes, C. E. Killian, P. Gilbert, A. Navrotsky, *Proc. Natl. Acad. Sci. USA* **2010**, *107*, 16438.
[11] a) Y. R. Ma, B. Aichmayer, O. Paris, P. Fratzl, A. Meibom, R. A. Metzler, Y. Politi, L. Addadi, P. Gilbert, S. Weiner, *Proc. Natl. Acad. Sci. USA* **2009**, *106*, 6048; b) P. Dubois, L. Ameye, *Microsc. Res. Tech.* **2001**, *55*, 427; c) V. Matranga, R. Bonaventura, C. Costa, K. Karakostis, A. Pinsino, R. Russo, F. Zito, *Mol. Biomineral.* **2011**, 225.
[12] C. E. Killian, F. H. Wilt, *Chem. Rev.* **2008**, *108*, 4463.
[13] A. Berman, J. Hanson, L. Leiserowitz, T. F. Koetzle, S. Weiner, L. Addadi, *Science* **1993**, *259*, 776.
[14] K. Okazaki, S. Inoue, *Dev. Growth Diff.* **1976**, *18*, 413.
[15] K. A. Guss, C. A. Ettensohn, *Development* **1997**, *124*, 1899.
[16] E. Beniash, L. Addadi, S. Weiner, *J. Struct. Biol.* **1999**, *125*, 50.
[17] P. Rez, A. Blackwell, *J. Phys. Chem. B* **2011**, *115*, 11193.
[18] F. H. Wilt, S. C. Benson, *Development of Sea Urchins, Ascidians, and Other Invertebrate Deuterostomes: Experimental Approaches*, Vol. *74*, Academic Press Inc., San Diego, CA **2004**, p. 273.
[19] L. S. Peck, A. C. Baker, L. Z. Conway, *J. Molluscan Stud.* **1996**, *62*, 315.
[20] L. E. Wasylenki, P. M. Dove, D. S. Wilson, J. J. De Yoreo, *Geochimi. Cosmochim. Acta* **2005**, *69*, 3017.
[21] E. Loste, R. M. Wilson, R. Seshadri, F. C. Meldrum, *J. Cryst. Growth* **2003**, *254*, 206.
[22] S. Weiner, L. Addadi, *Ann. Rev. Mater. Res.* **2011**, *41*, 21.
[23] A. A. Finch, N. Allison, *Mineral. Mag.* **2007**, *71*, 539.
[24] M. O. Krause, J. H. Oliver, *J. Phys. Chem. Ref. Data* **1979**, *8*, 329.
[25] T. Yamamoto, *X-Ray Spectrom.* **2008**, *37*, 572.
[26] R. W. G. Wyckoff, *Crystal Structures*, Vol. *2*, John Wiley & Sons, New York **1964**.
[27] R. D. Shannon, *Acta Crystallogr. Sect. A* **1976**, *32*, 751.
[28] B. Hasse, H. Ehrenberg, J. C. Marxen, W. Becker, M. Epple, *Chem.-Eur. J.* **2000**, *6*, 3679.
[29] a) P. Bots, L. G. Benning, J. D. Rodriguez-Blanco, T. Roncal-Herrero, S. Shaw, *Cryst. Growth Des.* **2012**, *12*, 3806; b) J. D. Rodriguez-Blanco, S. Shaw, L. G. Benning, *Nanoscale* **2011**, *3*, 265.
[30] N. Koga, Y. Z. Nakagoe, H. Tanaka, *Thermochim. Acta* **1998**, *318*, 239.
[31] N. E. Pingitore, F. W. Lytle, B. M. Davies, M. P. Eastman, P. G. Eller, E. M. Larson, *Geochim. Cosmochim. Acta* **1992**, *56*, 1531.
[32] a) C. Fahrni, *Curr. Opin. Chem. Biol.* **2007**, *11*, 121; b) P. Ingram, *Biomedical Applications of Microprobe Analysis*, Academic Press, San Diego, CA **1999**.
[33] M. R. Krejci, L. Finney , S. Vogt, D. Joester, *ChemSusChem* **2011**, *4*, 470.
[34] a) B. Ravel, M. Newville, *J. Synchrotron Radiat.* **2005**, *12*, 537 b) M. Newville, *J. Synchrotron Radiat.* **2001**, *8*, 322.
[35] B. Ravel, *J. Synchrotron Radiat.* **2001**, *8*, 314.